arXiv:1406.5522v1 [cond-mat.quant-gas] 20 Jun 2014

Three-body bound states in a harmonic waveguide with cylindrical symmetry

D. Blume[1, 2]

[1] *Department of Physics and Astronomy, Washington State University, Pullman, Washington 99164-2814, USA*
[2] *ITAMP, Harvard-Smithsonian Center for Astrophysics, 60 Garden Street, Cambridge, Massachusetts 02138, USA*

(Dated: June 24, 2014)

Highly-elongated quasi-one-dimensional cold atom samples have been studied extensively over the past years experimentally and theoretically. This work determines the energy spectrum of two identical fermions and a third distinguishable particle as functions of the mass ratio κ and the free-space s-wave scattering length a_{3D} between the identical fermions and the distinguishable third particle in a cylindrically symmetric waveguide whose symmetry axis is chosen to be along the z-axis. We focus on the regime where the mass of the identical fermions is equal to or larger than that of the third distinguishable particle. Our theoretical framework accounts explicitly for the motion along the transverse confinement direction. In the regime where excitations in the transverse direction are absent (i.e., for states with projection quantum number $M_{rel} = 0$), we determine the binding energies for states with odd parity in z. These full three-dimensional energies deviate significantly from those obtained within a strictly one-dimensional framework when the s-wave scattering length is of the order of or smaller than the oscillator length in the confinement direction. If transverse excitations are present, we predict the existence of a new class of universal three-body bound states with $|M_{rel}| = 1$ and positive parity in z. These bound states arise on the positive s-wave scattering length side if the mass ratio κ is sufficiently large. Implications of our results for ongoing cold atom experiments are discussed.

PACS numbers:

I. INTRODUCTION

Ultracold Bose and Fermi gases provide a unique environment for exploring few-body physics [1–4]. In the ultracold regime, the de Broglie wave length is much larger than the range of the underlying two-body potential, which implies that the details of the two-body interactions are, to a good approximation, negligible. To leading order, the interactions between two particles can be described by a single atomic physics parameter, the free-space s-wave scattering length a_{3D}. For a large number of atomic species, the s-wave scattering length can be tuned to essentially any value experimentally by varying an external magnetic field in the vicinity of a magnetic Fano-Feshbach resonance [5]. The ability to tune the s-wave scattering length to large positive and negative values, or even to zero, has opened the possibility to systematically map out the system behavior from the non-interacting regime to the weakly-attractive (weakly-repulsive) regime to the strongly-attractive (strongly-repulsive) regime [1, 6, 7].

The fact that the de Broglie wave length is, in the ultracold regime, much larger than the van der Waals length of atom-atom interactions justifies important simplifications in the theoretical treatment of cold atom gases. Specifically, the true atom-atom potential, which typically supports many two-body bound states, can be replaced by a simple model potential such as a zero-range pseudo-potential or a Gaussian potential, which supports at most a few two-body bound states. If the free-space scattering length of the model potential agrees with that of the true atom-atom potential, then theoretical treatments that utilize a model potential are, in general, expected to describe the low-energy physics with good accuracy.

This work determines the bound state spectrum of two identical fermions with mass m_h and a third distinguishable particle with mass m_l in a harmonic waveguide with cylindrical symmetry. The identical fermions interact through a simple two-body model potential with s-wave scattering length a_{3D} with the third distinguishable particle. Since the scattering between the identical fermions is, away from a p-wave resonance or higher partial wave resonances, suppressed by the Wigner threshold law, we assume that the identical fermions do not interact. We determine the bound state properties of this three-body system as functions of the interspecies s-wave scattering length a_{3D} and the mass ratio κ, where $\kappa = m_h/m_l$; we consider the regime $1 \leq \kappa \leq 12$. The bound state properties of fermionic three-body systems with unequal masses have previously been investigated in mixed dimensions [8, 9]. While atomic three-body systems in free space share many characteristics with the low-energy properties of few-nucleon systems [10], three-atom systems in a harmonic waveguide with cylindrical symmetry have no direct nuclear analog.

If transverse excitations are absent (i.e., if $M_{rel} = 0$) and if the size of the three-body bound state is much larger than the harmonic oscillator length a_{ho} that characterizes the confinement in the transverse direction, then a strictly one-dimensional Hamiltonian with appropriately chosen one-dimensional coupling constant provides a qualitatively correct description [11–15]. However, when the size of the three-body bound state becomes comparable to or smaller than a_{ho}, then the trimer

"feels" the full three-dimensional space and we find, in agreement with what might be expected naively, that a simple effective one-dimensional Hamiltonian provides a poor description. We also investigate the properties of states with $|M_{\rm rel}| = 1$ and positive parity in z. This case has, to the best of our knowledge, not been considered in the literature. At first sight, it may seem that the excitation in the transverse direction would prevent the formation of three-body bound states. Indeed, this is the case for mass ratios not much larger than one. For sufficiently large κ and positive s-wave scattering length, however, the attraction is sufficiently large to "outweigh" the energy increase due to the projection quantum number $M_{\rm rel}$ being finite. The existence of three-body bound states on the positive s-wave scattering length side is related to the fact that the three-body system in free space, i.e., in the absence of the waveguide, supports universal bound states with finite angular momentum if $\kappa \gtrsim 8.173$ and $a_{\rm 3D} > 0$ [16, 17]. Analogous effects have previously been studied in quasi-two-dimensional systems [18, 19]. Experimentally, the three-body bound states can potentially be probed via radio-frequency spectroscopy or detected via loss features due to three-body recombination processes. For K-Li mixtures [20–24], e.g., the three-body bound states should have profound effects on the system dynamics.

The remainder of this paper is organized as follows. Section II outlines the theoretical framework. Specifically, Sec. II A introduces the system Hamiltonian and discusses its symmetry properties; Sec. II B summarizes the numerical approach used to obtain the three-body spectra; and Sec. II C reviews a number of key results for two particles in a waveguide geometry. Section III discusses our results for different symmetries. Energy spectra are presented and the dependence of the energies on the range of the underlying two-body potential is analyzed. Lastly, Sec. IV summarizes.

II. THEORETICAL FRAMEWORK

A. System Hamiltonian and symmetries

We consider three particles with masses m_j and position vectors $\vec{r}_j = (x_j, y_j, z_j)$ in a cylindrically symmetric waveguide with angular trapping frequency ω. Assuming isotropic interactions $V_{\rm G}(r_{jk})$ ($r_{jk} = |\vec{r}_j - \vec{r}_k|$) between the distinguishable particles, the system Hamiltonian $H_{\rm tot}$ reads

$$H_{\rm tot} = \sum_{j=1}^{3} \left(\frac{-\hbar^2}{2m_j} \nabla^2_{\vec{r}_j} + \frac{1}{2} m_j \omega^2 \rho_j^2 \right) + \sum_{j=2}^{3} V_{\rm G}(r_{1j}), \quad (1)$$

where $\rho_j^2 = x_j^2 + y_j^2$. In Eq. (1), $\nabla^2_{\vec{r}_j}$ denotes the three-dimensional Laplacian of the jth particle. Our Hamiltonian assumes that the three particles with masses $m_1 = m_l$ and $m_2 = m_3 = m_h$ all feel the same angular trapping frequency. While this is fullfilled "automatically" for equal-mass systems, for unequal-mass systems the realization of equal trapping frequencies requires some fine-tuning [25]. In Eq. (1), $V_{\rm G}$ denotes a Gaussian model interaction potential with range r_0 and depth V_0 ($V_0 > 0$),

$$V_{\rm G}(r) = -V_0 \exp\left[-\left(\frac{r}{\sqrt{2} r_0} \right)^2 \right]. \quad (2)$$

For a fixed range r_0, V_0 is adjusted such that $V_{\rm G}$ supports no free-space bound state for $a_{\rm 3D} < 0$ and one free-space bound state for $a_{\rm 3D} > 0$. We work in the regime where r_0 is much smaller than the harmonic oscillator length $a_{\rm ho}$,

$$a_{\rm ho} = \sqrt{\frac{\hbar}{2\mu\omega}}, \quad (3)$$

where the two-body reduced mass μ is given by $m_h m_l/(m_h + m_l)$.

To analyze the symmetry properties of $H_{\rm tot}$, we introduce cylindrical coordinates, $(x_j, y_j, z_j) = (\rho_j \cos\varphi_j, \rho_j \sin\varphi_j, z_j)$. In these coordinates, we have $r_j^2 = \rho_j^2 + z_j^2$ and $r_{jk}^2 = \rho_{jk}^2 + z_{jk}^2$, where $\rho_{jk}^2 = (x_j - x_k)^2 + (y_j - y_k)^2$ and $z_{jk} = z_j - z_k$. It can be checked readily that $H_{\rm tot}$ is invariant under a rotation about the z-axis and when changing all x_j coordinates to $-x_j$ (and similarly for y_j and z_j). Correspondingly, we can find simultaneous eigenstates of $H_{\rm tot}$, the z-component of the orbital angular momentum operator $L_{{\rm tot},z}$, the parity operator P_z (P_z sends all z_j to $-z_j$), and the parity operator $P_{\vec{\rho}}$ ($P_{\vec{\rho}}$ sends all x_j to $-x_j$ and all y_j to $-y_j$).

Another important property of $H_{\rm tot}$ is that it can be written as a sum of the relative Hamiltonian $H_{\rm rel}$ and the center of mass Hamiltonian $H_{\rm cm}$,

$$H_{\rm tot} = H_{\rm rel} + H_{\rm cm}. \quad (4)$$

To write out $H_{\rm rel}$ and $H_{\rm cm}$, it is convenient to transform to Jacobi coordinates $\vec{r}_{\rm J1}$, $\vec{r}_{\rm J2}$ and $\vec{r}_{\rm J3}$ [$\vec{r}_{{\rm J}j} = (x_{{\rm J}j}, y_{{\rm J}j}, z_{{\rm J}j})$], where

$$\vec{r}_{\rm J1} = \vec{r}_1 - \vec{r}_2, \quad (5)$$

$$\vec{r}_{\rm J2} = \frac{m_1 \vec{r}_1 + m_2 \vec{r}_2}{m_1 + m_2} - \vec{r}_3 \quad (6)$$

and

$$\vec{r}_{\rm J3} = \frac{m_1 \vec{r}_1 + m_2 \vec{r}_2 + m_3 \vec{r}_3}{m_1 + m_2 + m_3}. \quad (7)$$

The center of mass Hamiltonian can be written in terms of $\vec{r}_{\rm J3}$ and the relative Hamiltonian $H_{\rm rel}$ in terms of $\vec{r}_{\rm J1}$ and $\vec{r}_{\rm J2}$.

In the following, we focus on solving the relative Schrödinger equation

$$H_{\rm rel} \Psi(\vec{r}_{\rm J1}, \vec{r}_{\rm J2}) = E_3 \Psi(\vec{r}_{\rm J1}, \vec{r}_{\rm J2}) \quad (8)$$

for the eigenstates Ψ with eigenenergy E_3. As before, we employ cylindrical coordinates, i.e., we write $\vec{r}_{\mathrm{J}j} = (\rho_{\mathrm{J}j}\cos\varphi_{\mathrm{J}j}, \rho_{\mathrm{J}j}\sin\varphi_{\mathrm{J}j}, z_{\mathrm{J}j})$ ($j = 1$ and 2). To take advantage of the Hamiltonian's symmetry, we perform an additional coordinate transformation, namely, we replace $\varphi_{\mathrm{J}1}$ and $\varphi_{\mathrm{J}2}$ by Φ and ϕ,

$$\Phi = \frac{1}{2}\left(\varphi_{\mathrm{J}1} + \varphi_{\mathrm{J}2}\right) \tag{9}$$

and

$$\phi = \varphi_{\mathrm{J}1} - \varphi_{\mathrm{J}2}. \tag{10}$$

It can be checked readily that the interaction potential is independent of the angle Φ. It follows that the relative wave function factorizes,

$$\Psi(\rho_{\mathrm{J}1}, \rho_{\mathrm{J}2}, \phi, \Phi, z_{\mathrm{J}1}, z_{\mathrm{J}2}) = \psi_{M_{\mathrm{rel}}}(\rho_{\mathrm{J}1}, \rho_{\mathrm{J}2}, \phi, z_{\mathrm{J}1}, z_{\mathrm{J}2})\exp(iM_{\mathrm{rel}}\Phi), \tag{11}$$

where $M_{\mathrm{rel}} = \cdots, -2, -1, 0, 1, 2, \cdots$. For $M_{\mathrm{rel}} \neq 0$, each eigenenergy is twofold degenerate due to the M_{rel} quantum number.

In the following, we label our solutions by the quantum numbers $\Pi_{\vec{\rho}}$, M_{rel} and Π_z, which are defined through the action of the operators $P_{\vec{\rho}}$, $L_{\mathrm{rel},z}$, and P_z on the eigenfunctions Ψ,

$$P_{\vec{\rho}}\Psi = \Pi_{\vec{\rho}}\Psi, \tag{12}$$

$$L_{\mathrm{rel},z}\Psi = \hbar M_{\mathrm{rel}}\Psi, \tag{13}$$

and

$$P_z\Psi = \Pi_z\Psi. \tag{14}$$

One finds $\Pi_{\vec{\rho}} = \pm 1$ [in fact, $\Pi_{\vec{\rho}} = (-1)^{M_{\mathrm{rel}}}$] and $\Pi_z = \pm 1$. For $M_{\mathrm{rel}} = 0$, we can find simultaneous eigenfunctions of H_{rel}, $P_{\vec{\rho}}$, $L_{\mathrm{rel},z}$, P_z and A_y, where the reflection operator A_y sends all y_j to $-y_j$ [26]. Specifically, for $M_{\mathrm{rel}} = 0$, we have

$$A_y\Psi = a_y\Psi \tag{15}$$

with $a_y = \pm 1$. We determine the relative eigenenergies E_3 and eigenstates Ψ [see Eq. (8)] by expanding Ψ in terms of explicitly correlated Gaussian basis functions with good $\Pi_{\vec{\rho}}$, M_{rel} and Π_z (and, if $M_{\mathrm{rel}} = 0$, a_y) quantum numbers and solve a generalized eigenvalue equation.

B. Explicitly correlated Gaussian basis set expansion approach

Explicitly correlated Gaussian basis functions have been shown to provide accurate descriptions of strongly-correlated systems such as nuclei, molecules, atoms, and quantum dots [27, 28]. They have also been employed to characterize small dilute atomic gases [28–31]. We write

$$\Psi(\vec{r}_{\mathrm{J}1}, \vec{r}_{\mathrm{J}2}) = \mathcal{A}\sum_{k=1}^{N_b} c_k f_k(x_{\mathrm{J}1}, y_{\mathrm{J}1}, x_{\mathrm{J}2}, y_{\mathrm{J}2}, \underline{A}_{\rho,k}, \vec{u}_{\rho,k}) \times g_k(z_{\mathrm{J}1}, z_{\mathrm{J}2}, \underline{A}_{z,k}, \vec{u}_{z,k}), \tag{16}$$

where $\mathcal{A}$ denotes the operator that ensures that the wave function is anti-symmetric under the exchange of the two identical fermions, $\mathcal{A} = 1 - P_{23}$ (P_{23} exchanges particles 2 and 3). The c_k denote expansion coefficients. These linear variational parameters are determined by solving the generalized eigenvalue problem defined by the Hamiltonian and overlap matrices. In Eq. (16), N_b denotes the size of the basis set. The functions f_k and g_k depend on a set of non-linear variational parameters through $\underline{A}_{\rho,k}$, $\vec{u}_{\rho,k}$, $\underline{A}_{z,k}$ and $\vec{u}_{z,k}$ [27, 32]. Here and in what follows, underlined symbols denote matrices.

We consider two different functional forms for g_k, one that is characterized by $\Pi_z = +1$ (referred to as $g_k^{(e)}$) and one that is characterized by $\Pi_z = -1$ (referred to as $g_k^{(o)}$),

$$g_k^{(e)}(z_{\mathrm{J}1}, z_{\mathrm{J}2}, \underline{A}_{z,k}) = \exp\left(-\frac{1}{2}\vec{z}_{\mathrm{J}}^{\,T}\,\underline{A}_{z,k}\vec{z}_{\mathrm{J}}\right) \tag{17}$$

and

$$g_k^{(o)}(z_{\mathrm{J}1}, z_{\mathrm{J}2}, \underline{A}_{z,k}, \vec{u}_{z,k}) = v_{z,k}\exp\left(-\frac{1}{2}\vec{z}_{\mathrm{J}}^{\,T}\,\underline{A}_{z,k}\vec{z}_{\mathrm{J}}\right), \tag{18}$$

where $\vec{z}_{\mathrm{J}} = (z_{\mathrm{J}1}, z_{\mathrm{J}2})$ and $\underline{A}_{z,k}$ denotes a symmetric 2×2 matrix. The quantity $v_{z,k}$ is defined through

$$v_{z,k} = \vec{u}_{z,k}^{\,T}\vec{z}_{\mathrm{J}}, \tag{19}$$

where $\vec{u}_{z,k}$ denotes a two-component vector. The elements of the vector $\vec{u}_{z,k}$ and the elements of the symmetric matrix $\underline{A}_{z,k}$ are treated as non-linear variational parameters [27, 32].

The functions f_k are characterized by the M_{rel} quantum number. For $M_{\mathrm{rel}} > 0$, we use [27]

$$f_k^{(M_{\mathrm{rel}})}(x_{\mathrm{J}1}, y_{\mathrm{J}1}, x_{\mathrm{J}2}, y_{\mathrm{J}2}, \underline{A}_{\rho,k}, \vec{u}_{\rho,k}) = (v_{x,k} + iv_{y,k})^{M_{\mathrm{rel}}}\exp\left(-\frac{1}{2}\vec{\rho}_{\mathrm{J}}^{\,T}\,\underline{A}_{\rho,k}\vec{\rho}_{\mathrm{J}}\right), \tag{20}$$

where $\vec{\rho}_{\mathrm{J}}$ is a two-component vector, $\vec{\rho}_{\mathrm{J}} = (\vec{\rho}_{\mathrm{J}1}, \vec{\rho}_{\mathrm{J}2})$, with the components being vector quantities themselves [$\vec{\rho}_{\mathrm{J}j} = (x_{\mathrm{J}j}, y_{\mathrm{J}j})$]. The 2×2 matrix $\underline{A}_{\rho,k}$ is symmetric; the independent elements of $\underline{A}_{\rho,k}$ are treated as non-linear variational parameters. The quantities $v_{x,k}$ and $v_{y,k}$ are defined through

$$v_{x,k} = \vec{u}_{\rho,k}^{\,T}\begin{pmatrix} x_{\mathrm{J}1} \\ x_{\mathrm{J}2}\end{pmatrix} \tag{21}$$

and

$$v_{y,k} = \vec{u}_{\rho,k}^{\,T}\begin{pmatrix} y_{\mathrm{J}1} \\ y_{\mathrm{J}2}\end{pmatrix}, \tag{22}$$

where $\vec{u}_{\rho,k}$ is a two-component vector whose components are treated as variational parameters. To understand the form of the prefactor of $f_k^{(M_{\rm rel})}$, we recall—using $x = \rho\cos\varphi$ and $y = \rho\sin\varphi$—that

$$[\rho\exp(i\varphi)]^{M_{\rm rel}} = (x+iy)^{M_{\rm rel}}. \tag{23}$$

The functions given in Eq. (20) describe states with $M_{\rm rel} > 0$. For the interaction model considered in this paper, the energy depends on $|M_{\rm rel}|$ and not the sign of $M_{\rm rel}$. Correspondingly, we only treat states with positive $M_{\rm rel}$.

To describe states with $M_{\rm rel} = 0$ and $a_y = +1$, we use [27]

$$f_k^{(0,+1)}(x_{\rm J1}, y_{\rm J1}, x_{\rm J2}, y_{\rm J2}, \underline{A}_{\rho,k}) = \exp\left(-\frac{1}{2}\vec{\rho}_{\rm J}^{\,T}\,\underline{A}_{\rho,k}\vec{\rho}_{\rm J}\right) \tag{24}$$

where the superscript indicates the $M_{\rm rel}$ and a_y quantum numbers. In this work, we do not report results for states with $(M_{\rm rel}, a_y) = (0,-1)$. States with this symmetry do not support three-body bound states if the range r_0 of the two-body potential is much smaller than $a_{\rm ho}$.

Compact analytical expressions for the Hamiltonian and overlap matrix elements can be obtained using the results of Ref. [27]. Our optimization procedure of the non-linear variational parameters is based on a semi-stochastic approach [32] and follows the scheme discussed in Ref. [31]. Our calculations reported in Sec. III use between 600 and 1300 basis functions. Each basis function is selected from around 4000-8000 trial functions. The resulting energies provide variational upper bounds for the exact ground state and excited state energies. The basis set extrapolation error depends on the system parameters and is at the sub-percent level or smaller.

Section III reports energies for the regime where r_0 is much smaller than $a_{\rm ho}$. In selected cases, the dependence of the energy on r_0 is investigated explicitly and the $r_0/a_{\rm ho} \to 0$ limit taken. From a numerical point of view, the presence of three, often vastly different, length scales (i.e., the harmonic oscillator length $a_{\rm ho}$, the range r_0 of the two-body potential, and the size of the bound state in the z-direction) is, in general, challenging. It has been shown in the literature that the basis functions employed in this work provide a reliable and efficient means to describe cold atom systems that are characterized by different length scales. Alternatively, one might employ zero-range interactions and solve the Lippmann-Schwinger equation [13–15].

C. Review: Two particles in a harmonic waveguide with cylindrical symmetry

To place the three-body study into context, this section reviews a number of key results for the two-body system in a harmonic waveguide with cylindrical symmetry. The system Hamiltonian is given by Eq. (1) with the first and second sum in Eq. (1) running from $j = 1$ to 2 and from $j = 2$ to 2, respectively (instead of from $j = 1$ to 3 and from $j = 2$ to 3). Separating off the center of mass motion, the problem reduces to that of a reduced mass particle that feels a spherically symmetric short-range potential with s-wave scattering length $a_{\rm 3D}$. In the zero-range limit, i.e., for $r_0 = 0$, the two-body scattering and bound state solutions have been determined analytically in the seminal work by Olshanii [11]. Importantly, if the one-dimensional coupling constant g (see below) and the relative two-body energy are, for a fixed interaction potential, scaled by $\hbar\omega a_{\rm ho}$ and $\hbar^2/(2\mu a_{\rm ho}^2)$, respectively, then these quantities are independent of the mass ratio κ.

The outcome of a scattering event between the two particles in the $(\Pi_{\vec{\rho}}, M_{\rm rel}, \Pi_z, a_y) = (+1, 0, +1, +1)$ channel is, for $r_0 = 0$, characterized by the effective one-dimensional even parity coupling constant g [11],

$$\frac{g}{\hbar\omega_\rho\, a_{\rm ho}} = \frac{2a_{\rm 3D}}{a_{\rm ho}}\left(1 + \frac{\zeta(1/2)}{\sqrt{2}}\frac{a_{\rm 3D}}{a_{\rm ho}}\right)^{-1}, \tag{25}$$

where $\zeta(1/2) \approx -1.46035$. Equation (25) shows that the one-dimensional coupling constant depends on the ratio $a_{\rm 3D}/a_{\rm ho}$. This implies that it can be tuned either by varying the harmonic oscillator length of the waveguide or by varying the three-dimensional s-wave scattering length through application of an external magnetic field in the vicinity of a Fano-Feshbach resonance. Specifically, the one-dimensional coupling constant g diverges when the s-wave scattering length takes the value $a_{\rm 3D} \approx 1.03263 a_{\rm ho}$. The solid line in Fig. 1(a) shows the quantity $(\hbar\omega a_{\rm ho})/g$ as a function of $a_{\rm ho}/a_{\rm 3D}$.

While the two-body system in free space supports a weakly-bound state only for positive s-wave scattering length, the waveguide supports a two-body bound state with $(\Pi_{\vec{\rho}}, M_{\rm rel}, \Pi_z, a_y) = (+1, 0, +1, +1)$ symmetry for all $a_{\rm 3D}$ [11, 12]. Note that the two-body system is bound if its relative energy is less than $\hbar\omega$, i.e., if its relative energy is less than the zero-point energy of the reduced mass particle in a two-dimensional harmonic oscillator. The relative binding energy E_2 is, for zero-range interactions, determined by the implicit eigenvalue equation [11, 12]

$$\frac{1}{\sqrt{2}}\zeta\left(\frac{1}{2}, -\frac{E_2}{2\hbar\omega} + \frac{1}{2}\right) = -\frac{a_{\rm ho}}{a_{\rm 3D}}, \tag{26}$$

where $\zeta(\cdot,\cdot)$ denotes the Hurwitz zeta function. The solution is shown by the solid line in Fig. 1(b) as a function of $a_{\rm ho}/a_{\rm 3D}$. For comparison, dashed and dotted lines show the relative binding energy for the Gaussian model potential with $r_0 = 0.005 a_{\rm ho}$ and $0.01 a_{\rm ho}$, respectively. These two-body binding energies are obtained by solving the relative two-dimensional Schrödinger equation using B-splines and are used in Sec. III to analyze the three-body spectra. The finite-range effects increase as $a_{\rm ho}/a_{\rm 3D}$ increases. For $a_{\rm ho}/a_{\rm 3D} = 10$, e.g., the finite-range energies deviate from the zero-range energy by -11% and -24% for $r_0 = 0.005 a_{\rm ho}$ and $r_0 = 0.01 a_{\rm ho}$, respectively. The

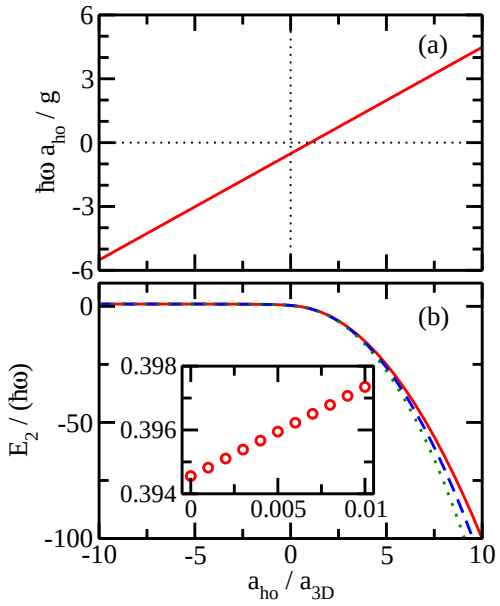

FIG. 1: (Color online) Coupling constant and binding energy for two particles in a harmonic waveguide with cylindrical symmetry. (a) The solid line shows the inverse of the effective one-dimensional coupling constant g [see Eq. (25)] as a function of $a_{\rm ho}/a_{\rm 3D}$ for $r_0 = 0$. (b) The solid line shows the relative two-body binding energy E_2 [see Eq. (26)] as a function of $a_{\rm ho}/a_{\rm 3D}$ for $r_0 = 0$. For $a_{\rm ho}/a_{\rm 3D} \to -\infty$, E_2 approaches $\hbar\omega$. For comparison, dashed and dotted lines show E_2 for $r_0 = 0.005 a_{\rm ho}$ and $0.01 a_{\rm ho}$, respectively. Inset: Symbols show $E_2/(\hbar\omega)$ as a function of $r_0/a_{\rm ho}$ for $a_{\rm ho}/a_{\rm 3D} = 0$.

inset of Fig. 1(b) shows the two-body binding energy as a function of $r_0/a_{\rm ho}$ for $a_{\rm ho}/a_{\rm 3D} = 0$. For this scattering length, the finite-range energies lie (slightly) above the zero-range energy. For sufficienty small r_0, channels with $M_{\rm rel} > 0$ and/or $\Pi_z = -1$ do not support a two-body bound state for any $a_{\rm 3D}$.

III. THREE-BODY BOUND STATES

A. General considerations

This section summarizes our search for three-body bound states in a waveguide with cylindrical symmetry. Throughout, we focus on parameter combinations for which $|a_{\rm 3D}| \gg r_0$ and $a_{\rm ho} \gg r_0$. As discussed in Sec. II C, the two-body system with short-range interactions supports a bound state with relative energy E_2 for all $a_{\rm 3D}$. This work investigates under which conditions the three-body system supports states that are stable with respect to the lowest dimer plus atom threshold, i.e., whose relative energy E_3 is smaller than $E_2 + \hbar\omega$. The addition of the third particle has two effects: *(i)* The interaction potential $V_{\rm G}(r_{13})$ introduces an additional attraction. *(ii)* The fact that the three-particle wave function has to be anti-symmetric under the exchange of particles 2 and 3 introduces an effective repulsion. Whether or not three-body bound states exist is determined by the interplay of these two effects.

For equal masses, the three-body bound states in a waveguide have been characterized in Refs. [13, 14]. For unequal masses, the bound states of three particles in a waveguide have been investigated within a strictly one-dimensional framework, in which the unlike particles interact through a one-dimensional δ-function potential with effective coupling constant g [33–35], and not yet within a full three-dimensional framework. It was found that three-body bound states are only supported if g is negative, corresponding to $a_{\rm ho}/a_{\rm 3D} \lesssim 1/1.03263 \approx 0.96840$, $\Pi_z = -1$ and $\kappa > 1$. Specifically, if κ is infinitesimally larger than 1, an infinitesimally weakly-bound three-body state emerges for $g \to -\infty$. For $\kappa \approx 7.3791$, a second three-body bound state becomes bound.

In addition to this one-dimensional limit, the bound states of the three-body system in free space [i.e., in the case where the waveguide is absent ($\omega \to 0$)] are known [16]. In this case, a universal three-body bound state with $(L, \Pi) = (1, -1)$ symmetry exists if $\kappa \gtrsim 8.173$ and $a_{\rm 3D} > 0$ [16]; here, L denotes the relative orbital angular momentum of the three-body system and Π the parity. In the limit that the three-dimensional scattering length $a_{\rm 3D}$ is smaller than the harmonic oscillator length $a_{\rm ho}$ that characterizes the waveguide, we expect that the three-body solutions for the waveguide system show similarities with those for the free-space system. In this limit, the waveguide can be thought of as introducing a small perturbation to the free-space solution. Correspondingly, we expect that three-body bound states exist for sufficiently large κ, if the symmetry of the waveguide solution is "consistent" with the $(L, \Pi) = (1, -1)$ symmetry of the free-space solution that supports a universal three-body bound state.

Section III B summarizes our results for $\kappa = 1$. Our full three-dimensional calculations for $\kappa = 1$ confirm, as suggested by Refs. [13, 14, 34], the absence of three-body bound states in the $(\Pi_{\vec\rho}, M_{\rm rel}, \Pi_z, a_y) = (+1, 0, \pm 1, +1)$ channels. Our calculations for $\kappa > 1$ are summarized in Secs. III C-III E: Section III C discusses our results for the $(\Pi_{\vec\rho}, M_{\rm rel}, \Pi_z, a_y) = (+1, 0, +1, +1)$ channel, Sec. III D those for the $(\Pi_{\vec\rho}, M_{\rm rel}, \Pi_z, a_y) = (+1, 0, -1, +1)$ channel, and Sec. III E those for the $(\Pi_{\vec\rho}, |M_{\rm rel}|, \Pi_z) = (-1, 1, +1)$ channel. We find that the $(\Pi_{\vec\rho}, M_{\rm rel}, \Pi_z, a_y) = (+1, 0, -1, +1)$ and $(\Pi_{\vec\rho}, |M_{\rm rel}|, \Pi_z) = (-1, 1, +1)$ channels support three-body bound states in certain regions of the parameter space. These channels have an overall negative parity, i.e., $\Pi_{\vec\rho} \times \Pi_z = -1$, and are thus "consistent" with the free-space solution that has $(L, \Pi) = (1, -1)$ symmetry and supports universal three-body bound states for sufficiently large κ and positive $a_{\rm 3D}$.

B. Absence of three-body bound states for $\kappa = 1$

For equal masses (i.e., for $\kappa = 1$), we find that the Pauli exclusion principle outweighs the energy decrease due to the attraction. Specifically, for $\kappa = 1$, $r_0 = 0.01a_{\rm ho}$ and $a_{\rm ho}/a_{\rm 3D} \in [-10, 10]$, we determined the three-body energies using the approach discussed in Sec. II B and found that the $(\Pi_{\vec{\rho}}, M_{\rm rel}, \Pi_z, a_y) = (+1, 0, \pm 1, +1)$ and $(\Pi_{\vec{\rho}}, |M_{\rm rel}|, \Pi_z) = (-1, 1, +1)$ channels do not support three-body bound states. For a subset of scattering lengths, we decreased the range r_0 of the Gaussian model potential and found no significant change. We thus believe that three-body bound states are absent also in the zero-range limit.

C. $(\Pi_{\vec{\rho}}, M_{\rm rel}, \Pi_z, a_y) = (+1, 0, +1, +1)$

Considering mass ratios up to $\kappa = 12$ and inverse scattering lengths $a_{\rm ho}/a_{\rm 3D}$ ranging from -10 to 10, we found no three-body bound states in the $(\Pi_{\vec{\rho}}, M_{\rm rel}, \Pi_z, a_y) = (+1, 0, +1, +1)$ channel. Although the calculations were performed for a finite range (namely for $r_0 = 0.01a_{\rm ho}$), we believe that the results also hold for three-body systems with zero-range interactions. This finding is consistent with the results obtained within the strictly-one-dimensional framework [34]. Moreover, the absence of three-body bound states in the $(\Pi_{\vec{\rho}}, M_{\rm rel}, \Pi_z, a_y) = (+1, 0, +1, +1)$ channel for large $a_{\rm ho}/a_{\rm 3D}$ is consistent with the fact that the free-space system with positive parity does not support three-body bound states [36–39].

D. $(\Pi_{\vec{\rho}}, M_{\rm rel}, \Pi_z, a_y) = (+1, 0, -1, +1)$

Figure 2 shows the three-body energies for the lowest state with $(\Pi_{\vec{\rho}}, M_{\rm rel}, \Pi_z, a_y) = (+1, 0, -1, +1)$ symmetry as a function of $a_{\rm ho}/a_{\rm 3D}$ for various mass ratios. The results are obtained for $r_0 = 0.01a_{\rm ho}$. As mentioned above, three-body states are bound with respect to the breakup into a dimer and an atom if their energy is less than $E_2 + \hbar\omega$. Correspondingly, Fig. 2 shows the quantity $(E_3 - E_2 - \hbar\omega)/(\hbar\omega)$.

For $r_0 = 0.01a_{\rm ho}$, the system with $\kappa = 3/2$ supports three-body bound states with binding energies around $-6.5 \times 10^{-5}\hbar\omega$ and $-2 \times 10^{-4}\hbar\omega$ (these are variational upper bounds) for $a_{\rm ho}/a_{\rm 3D} = -1.5$ and -1, respectively. For the range of $r_0 = 0.01a_{\rm ho}$, we find no three-body bound states for $a_{\rm ho}/a_{\rm 3D} = -2$ and -0.5. While the exact threshold scattering lengths, i.e., the scattering lengths at which the system becomes unbound, depend on the range of the underlying two-body potential, our results confirm the existence of weakly-bound states for $\kappa > 1$.

For larger mass ratios, the scattering length window for which three-body bound states are supported increases, especially on the negative scattering length side. On the positive scattering length side, the bound state region also increases. For $\kappa = 5$, e.g., three-body bound states are supported for positive g (i.e., for $a_{\rm ho}/a_{\rm 3D} \gtrsim 1/1.03263$). To see if this is a consequence of the finite-range nature of the interactions, Figs. 3(a) and 3(b) show the scaled three-body energy $(E_3 - E_2)/(\hbar\omega)$ as a function of r_0 for $a_{\rm ho}/a_{\rm 3D} = 1$ and $a_{\rm ho}/a_{\rm 3D} = 2$, respectively. Although the binding energy decreases with decreasing range, Fig. 3 shows that the three-body system is bound for all r_0 considered, including the zero-range limit. This implies that three-body bound states are, for sufficiently large κ, not only supported if g is negative but also if g is positive. This is in contrast to the prediction based on the purely one-dimensional framework [34], where a positive g corresponds to a purely repulsive system. The strictly one-dimensional treatment could be improved, as suggested in Refs. [11, 12], by using the energy-dependent Hurwitz zeta function instead of the energy-independent zeta function in the parametrization of the one-dimensional coupling constant g [see Eq. (25)].

To determine whether the three-body bound states are universal for larger κ and large $|a_{\rm 3D}|$, Figs. 4(a) and 4(b) show the range dependence of the scaled three-body energy for $a_{\rm ho}/a_{\rm 3D} = 0$ as a function of r_0 for $\kappa = 6$ and 10, respectively. The range dependence is quite

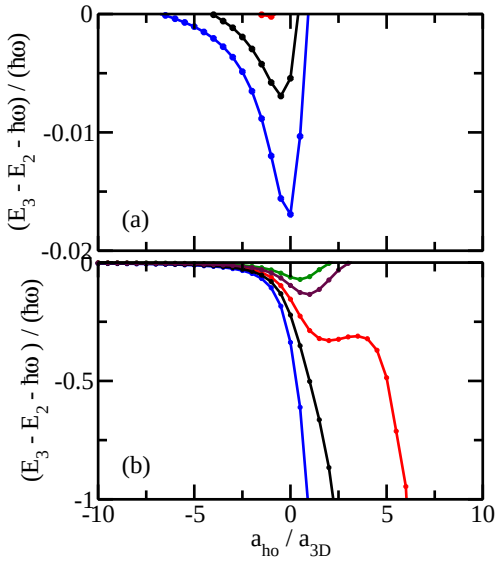

FIG. 2: (Color online) Relative three-body energies for the lowest state with $(\Pi_{\vec{\rho}}, M_{\rm rel}, \Pi_z, a_y) = (+1, 0, -1, +1)$ symmetry as a function of $a_{\rm ho}/a_{\rm 3D}$. (a) The symbols show the dimensionless energy difference $(E_3 - E_2 - \hbar\omega)/(\hbar\omega)$ for $\kappa = 3/2$ (top curve; exists only around $a_{\rm ho}/a_{\rm 3D} = -1$), $\kappa = 2$ (middle curve) and $\kappa = 5/2$ (bottom curve). (b) The symbols show the dimensionless energy difference $(E_3 - E_2 - \hbar\omega)/(\hbar\omega)$ for $\kappa = 4$ (top curve), 5, 13/2, 8, and 10 (bottom curve). The lines connect the data points as a guide to the eye. The calculations are performed for $r_0 = 0.01a_{\rm ho}$.

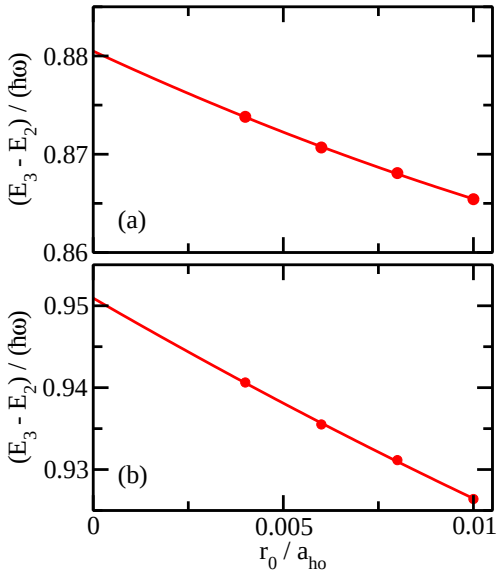

FIG. 3: (Color online) Range dependence of the relative three-body energy of the lowest state with $(\Pi_{\vec{\rho}}, M_{\rm rel}, \Pi_z, a_y) = (+1, 0, -1, +1)$ symmetry and $\kappa = 5$. The symbols show the dimensionless energy difference $(E_3 - E_2)/(\hbar\omega)$ for (a) $a_{\rm ho}/a_{\rm 3D} = 1$ and (b) $a_{\rm ho}/a_{\rm 3D} = 2$. The lines show three parameter fits to the scaled finite-range energies.

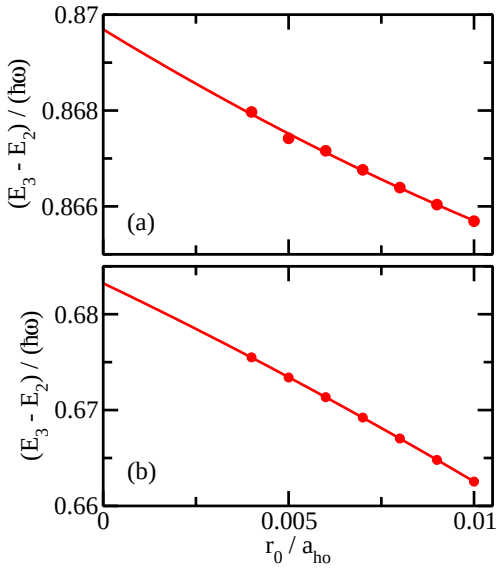

FIG. 4: (Color online) Range dependence of the relative three-body energy of the lowest state with $(\Pi_{\vec{\rho}}, M_{\rm rel}, \Pi_z, a_y) = (+1, 0, -1, +1)$ symmetry and $a_{\rm ho}/a_{\rm 3D} = 0$. The symbols show the dimensionless energy difference $(E_3 - E_2)/(\hbar\omega)$ for (a) $\kappa = 6$ and (b) $\kappa = 10$. The lines show three parameter fits to the scaled finite-range energies.

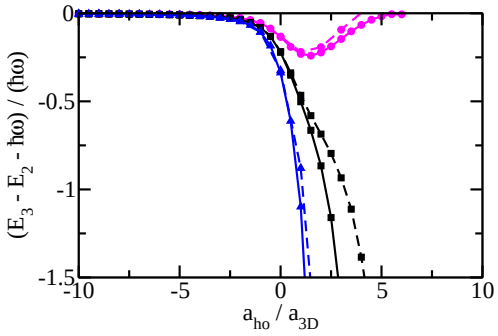

FIG. 5: (Color online) Range-dependence of the relative three-body energies for the lowest state with $(\Pi_{\vec{\rho}}, M_{\rm rel}, \Pi_z, a_y) = (+1, 0, -1, +1)$ symmetry as a function of $a_{\rm ho}/a_{\rm 3D}$. The circles, squares and triangles show the dimensionless energy difference $(E_3 - E_2 - \hbar\omega)/(\hbar\omega)$ for $\kappa = 6, 8$ and 10, respectively. The dimensionless energies are connected by dashed and solid lines for $r_0 = 0.005 a_{\rm ho}$ and $0.01 a_{\rm ho}$, respectively.

small even for these large mass ratios, suggesting that the three-body bound states in the $(\Pi_{\vec{\rho}}, M_{\rm rel}, \Pi_z, a_y) = (+1, 0, -1, +1)$ channel are rather insensitive to the details of the underlying two-body potential if $a_{\rm ho}/a_{\rm 3D} \ll 1$, $a_{\rm ho}/r_0 \gg 1$ and $|a_{\rm 3D}|/r_0 \gg 1$. In the regime where $a_{\rm ho}/a_{\rm 3D} \gg 1$, however, the finite-range effects are notably more important. As an example, Fig. 5 compares the scaled energy $(E_3 - E_2 - \hbar\omega)/(\hbar\omega)$ for $r_0 = 0.01 a_{\rm ho}$ (solid lines) and $r_0 = 0.005 a_{\rm ho}$ (dashed lines) for $\kappa = 6, 8$ and 10. While the qualitative behavior is independent of r_0, quantitative differences are visible in the $a_{\rm ho} > a_{\rm 3D}$ regime.

Lastly, we search for excited states in the $(\Pi_{\vec{\rho}}, M_{\rm rel}, \Pi_z, a_y) = (+1, 0, -1, +1)$ channel. As discussed above, the strictly one-dimensional framework predicts that excited states are supported if κ is greater than 7.3791 [34]. For $\kappa = 8$ and $r_0 = 0.01 a_{\rm ho}$, we found that the first excited state is, within our variational treatment, not bound with respect to the break-up into a dimer and an atom. We did not investigate how this "negative result" depends on the range of the underlying two-body potential. For $\kappa = 9$, however, the system supports an excited three-body bound state, as expected from the strictly one-dimensional framework. Circles in Fig. 6 show the scaled energy of the first excited state as a function of $a_{\rm ho}/a_{\rm 3D}$ for $\kappa = 9$ and $r_0 = 0.01 a_{\rm ho}$. The dependence of the excited states on the s-wave scattering length seems to be similar to that of the ground state (compare Fig. 6 with Figs. 2 and 5).

E. $(\Pi_{\vec{\rho}}, |M_{\rm rel}|, \Pi_z) = (-1, 1, +1)$

This section explores under which conditions the three-body system in the $(\Pi_{\vec{\rho}}, |M_{\rm rel}|, \Pi_z) = (-1, 1, +1)$ chan-

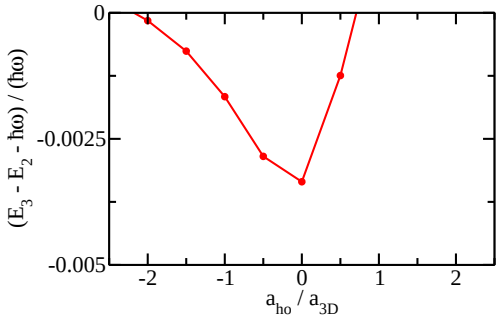

FIG. 6: (Color online) Relative energy of the first excited three-body state with $(\Pi_{\vec{\rho}}, M_{\rm rel}, \Pi_z, a_y) = (+1, 0, -1, +1)$ symmetry as a function of $a_{\rm ho}/a_{\rm 3D}$. The symbols show the scaled energy $(E_3 - E_2 - \hbar\omega)/(\hbar\omega)$ for $\kappa = 9$ and $r_0 = 0.01 a_{\rm ho}$. Lines connect the data points as a guide to the eye.

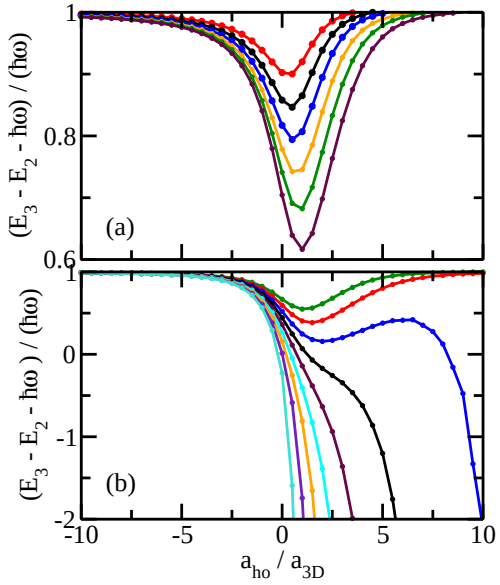

FIG. 7: (Color online) Relative three-body energies for the lowest state with $(\Pi_{\vec{\rho}}, |M_{\rm rel}|, \Pi_z) = (-1, 1, +1)$ symmetry as a function of $a_{\rm ho}/a_{\rm 3D}$. (a) Symbols show the dimensionless energy difference $(E_3 - E_2 - \hbar\omega)/(\hbar\omega)$ for $\kappa = 1$ (top curve), 3/2, 2, 5/2, 3 and 7/2 (bottom curve). (b) The symbols show the dimensionless energy difference $(E_3 - E_2 - \hbar\omega)/(\hbar\omega)$ for $\kappa = 4$ (top curve), 5, 6, 7, 8, 9, 10, 11 and 12 (bottom curve). The lines connect the data points as a guide to the eye. The calculations are performed for $a_0 = 0.01 a_{\rm ho}$.

nel supports bound states that are stable with respect to the lowest dimer plus atom threshold with energy $E_2 + \hbar\omega$. Figure 7 shows the dimensionless energy $(E_3 - E_2 - \hbar\omega)/(\hbar\omega)$ for $r_0 = 0.01 a_{\rm ho}$ as a function of $a_{\rm ho}/a_{\rm 3D}$ for various κ. For $\kappa = 1$ [top curve in Fig. 7(a)], the scaled energy $(E_3 - E_2 - \hbar\omega)/(\hbar\omega)$ shows a minimum

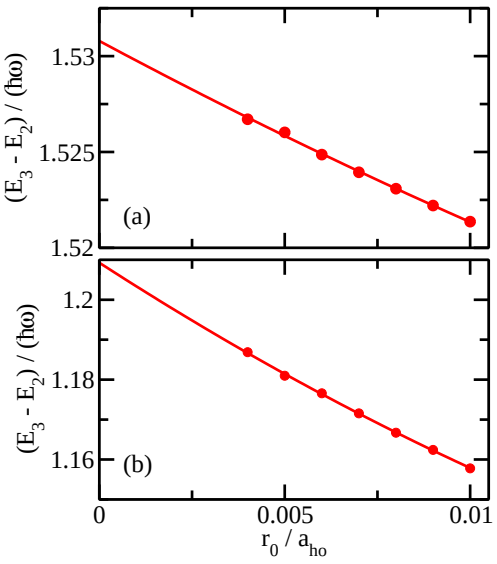

FIG. 8: (Color online) Range dependence of the relative three-body energy of the lowest state with $(\Pi_{\vec{\rho}}, |M_{\rm rel}|, \Pi_z) = (-1, 1, +1)$ symmetry and $a_{\rm ho}/a_{\rm 3D} = 0$. The symbols show the dimensionless energy difference $(E_3 - E_2)/(\hbar\omega)$ for (a) $\kappa = 6$ and (b) $\kappa = 10$. The solid lines show three parameter fits to the scaled finite-range energies.

near $a_{\rm ho}/a_{\rm 3D} = 0$. As κ increases, the minimum deepens and moves slightly to the positive scattering length side. While these systems with κ not much larger than 1 are bound with respect to the excited dimer plus atom threshold with energy $E_2 + 2\hbar\omega$, they are not bound with respect to the lowest dimer plus atom threshold with energy $E_2 + \hbar\omega$. For $\kappa = 6$ [third curve from the top in Fig. 7(b)], the scaled energy $(E_3 - E_2 - \hbar\omega)/(\hbar\omega)$ drops below -1 for large $a_{\rm ho}/a_{\rm 3D}$. For yet larger κ, the scaled energy $(E_3 - E_2 - \hbar\omega)/(\hbar\omega)$ decreases monotonically with increasing $a_{\rm ho}/a_{\rm 3D}$. For $\kappa = 8 - 12$, the three-body system with $r_0 = 0.01 a_{\rm ho}$ becomes bound with respect to the lowest dimer plus atom threshold for $a_{\rm ho}/a_{\rm 3D}$ between approximately 3 to 0.5.

To investigate the range dependence of the three-body energies, Figs. 8(a) and 8(b) show the energy difference $(E_3 - E_2)/(\hbar\omega)$ for $a_{\rm ho}/a_{\rm 3D} = 0$ as a function of r_0 for $\kappa = 6$ and $\kappa = 10$, respectively. The energy difference depends approximately linearly on the range. Figures 8(a) and 8(b) show that the range dependence increases with increasing κ.

To obtain a sense of the range dependence on the negative scattering length side, Fig. 9(a) shows the difference between the three-body energies for $r_0 = 0.01 a_{\rm ho}$ and $r_0 = 0.005 a_{\rm ho}$ for $\kappa = 6$ (circles), $\kappa = 8$ (squares) and $\kappa = 10$ (triangles). The range dependence is very small on the negative scattering length side. To visualize

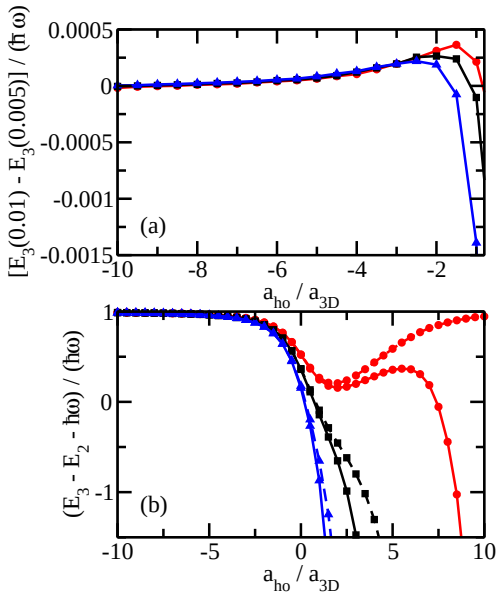

FIG. 9: (Color online) Range dependence of the relative three-body energy of the lowest state with $(\Pi_{\vec{\rho}}, |M_{\rm rel}|, \Pi_z) = (-1, 1, +1)$ symmetry as a function of $a_{\rm ho}/a_{\rm 3D}$. (a) The circles, squares and triangles show the energy difference $[E_3(r_0 = 0.01a_{\rm ho}) - E_3(r_0 = 0.005a_{\rm ho})]/(\hbar\omega)$ for $\kappa = 6$, 8 and 10, respectively. The lines connect the data points as a guide to the eye. (b) The circles, squares and triangles show the quantity $(E_3 - E_2 - \hbar\omega)/(\hbar\omega)$ for $\kappa = 6$, 8 and 10. The dimensionless energies are connected by dashed and solid lines for $r_0 = 0.005a_{\rm ho}$ and $r_0 = 0.01a_{\rm ho}$, respectively.

the range dependence in the strongly interacting regime (including the positive scattering length side), Fig. 9(b) shows the scaled energies $(E_3 - E_2 - \hbar\omega)/(\hbar\omega)$ for two different ranges, $r_0 = 0.01a_{\rm ho}$ and $r_0 = 0.005a_{\rm ho}$, and three mass ratios, $\kappa = 6$, 8 and 10. Roughly speaking, the range of the two-body potential becomes important when $a_{\rm ho}/a_{\rm 3D} \gtrsim -1$.

As pointed out earlier, the states with $(\Pi_{\vec{\rho}}, |M_{\rm rel}|, \Pi_z) = (-1, 1, +1)$ symmetry considered here are consistent with the $(L, \Pi) = (1, -1)$ symmetry of the three-dimensional free-space system. For mass ratios $\kappa > 8.173$ and zero-range interactions, the energy of the free-space system in the $(1, -1)$ channel is directly proportional to $(a_{\rm 3D})^{-2}$. Thus we expect that the three-body energies for the wave guide Hamiltonian for positive $a_{\rm 3D}$ scale in the same way. We find that this is only approximately true for the parameter regime explored in this work. The requirement that $a_{\rm 3D}$ should be less than $a_{\rm ho}$ and larger than r_0, combined with large finite range effects, make it challenging, at least for the numerical approach employed in this work, to reach the regime where the energies for the wave guide Hamiltonian approach those for the free-space Hamiltonian with zero-range interactions.

IV. SUMMARY

This paper determined the bound states of two identical heavy fermions and one light particle in a harmonic waveguide for short-range interspecies s-wave interactions. Our calculations accounted for the full dynamics along the direction of the harmonic confinement as well as along the direction of the waveguide, i.e., coupling between the degrees of freedom along these directions was treated explicitly. Comparisons with predictions based on an effective one-dimensional Hamiltonian were presented. We investigated three different symmetries:

(i) For states with $(\Pi_{\vec{\rho}}, |M_{\rm rel}|, \Pi_z, a_y) = (+1, 0, +1, +1)$ symmetry, no three-body bound states were found for the mass ratios investigated. This finding is in agreement with what is expected based on results for an effective one-dimensional Hamiltonian and the three-dimensional free-space results for $(L, \Pi) = (0, +1)$ symmetry.

(ii) For states with $(\Pi_{\vec{\rho}}, |M_{\rm rel}|, \Pi_z, a_y) = (+1, 0, -1, +1)$ symmetry, three-body bound states were found for $\kappa > 1$ in the strongly-interacting regime. For sufficiently large κ, three-body bound states exist not only on the negative scattering length side but also on the positive scattering length side. While the bound states on the positive scattering length side are absent in the strictly one-dimensional treatment, their existence for sufficiently large κ is expected since free-space systems with $(L, \Pi) = (1, -1)$ symmetry support universal three-body states for positive $a_{\rm 3D}$ and $\kappa > 8.173$ [16].

(iii) For states with $(\Pi_{\vec{\rho}}, |M_{\rm rel}|, \Pi_z) = (-1, 1, +1)$ symmetry, three-body bound states were found for sufficiently large κ. This is a new class of bound states that has, to the best of our knowledge, not been considered before. The anti-symmetry of the corresponding eigenstates is ensured by placing an excitation into the angular degrees of freedom, allowing the solution along the waveguide axis to have positive parity (i.e., $\Pi_z = +1$) and no nodes. The three-body bound state first emerges on the positive scattering length side.

A variety of unequal-mass systems have been trapped and cooled to the degenerate or near-degenerate regime over the past 10 years or so, and the creation of effectively one-dimensional confining geometries is fairly standard by now. Recent experiments on K-Li mixtures with mass ratio $\kappa \approx 6.5$ [24], e.g., investigated the effects of the $L = 1$ states on the positive s-wave scattering length side on the collision dynamics in the three-dimensional regime. It would be very interesting to extend these experimental studies to the effectively one-dimensional regime, where the strength of the confinement can be used to tune the interaction strength. By changing ω, the ratio $a_{\rm ho}/a_{\rm 3D}$ and, correspondingly, the position of the three-body bound state relative to the lowest dimer plus atom threshold can be tuned. It would be interesting to monitor the three-body recombination rate and to thus indirectly search for signatures of the three-body bound

states in the $(\Pi_{\vec{\rho}}, |M_{\rm rel}|, \Pi_z, a_y) = (+1, 0, -1, +1)$ and $(\Pi_{\vec{\rho}}, |M_{\rm rel}|, \Pi_z) = (-1, 1, +1)$ channels. Alternatively, it would be interesting to probe the three-body bound states directly by radio-frequency spectroscopy. In the future, it will be interesting to extend the studies presented here to other confinement geometries, to other particle symmetries and to larger systems.

Acknowledgement: DB is grateful to Janine Shertzer for extensive discussions involving the symmetry of the Hamiltonian and for preliminary calculations of effective hyperradial potential curves using a 4D finite element analysis. DB also thanks Debraj Rakshit and Ebrahim Gharashi for helpful discussions, and acknowledges support by the NSF through grant PHY-1205443. This work was additionally supported by the National Science Foundation through a grant for the Institute for Theoretical Atomic, Molecular and Optical Physics at Harvard University and Smithsonian Astrophysical Observatory.

[1] D. Blume. Progress in Physics **75**, 046401 (2012).
[2] E. Braaten and H.-W. Hammer. Phys. Rep. **428**, 259 (2006).
[3] C. H. Greene. Physics Today **63**, 40 (2010).
[4] F. Ferlaino and R. Grimm. Physics **3**, 9 (2010).
[5] C. Chin, R. Grimm, P. Julienne, and E. Tiesinga. Rev. Mod. Phys. **82**, 1225 (2010).
[6] S. Giorgini, L. P. Pitaevskii, and S. Stringari. Rev. Mod. Phys. **80**, 1215 (2008).
[7] I. Bloch, J. Dalibard, and W. Zwerger. Rev. Mod. Phys. **80**, 885 (2008).
[8] Y. Nishida and S. Tan. Phys. Rev. Lett. **101**, 170401 (2008).
[9] T. Yin, P. Zhang, and W. Zhang. Phys. Rev. A **84**, 052727 (2011).
[10] H.-W. Hammer, A. Nogga, and A. Schwenk. Rev. Mod. Phys. **85**, 197 (2013).
[11] M. Olshanii. Phys. Rev. Lett. **81**, 938 (1998).
[12] T. Bergeman, M. G. Moore, and M. Olshanii. Phys. Rev. Lett. **91**, 163201 (2003).
[13] C. Mora, R. Egger, A. O. Gogolin, and A. Komnik. Phys. Rev. Lett. **93**, 170403 (2004).
[14] C. Mora, R. Egger, and A. O. Gogolin. Phys. Rev. A **71**, 052705 (2005).
[15] S. E. Gharashi, K. M. Daily, and D. Blume. Phys. Rev. A **86**, 042702 (2012).
[16] O. I. Kartavtsev and A. V. Malykh. J. Phys. B **40**, 1429 (2007).
[17] S. Endo, P. Naidon and M. Ueda. Few-Body Systems **51**, 207 (2011).
[18] J. Levinsen, T. G. Tiecke, J. T. M. Walraven, and D. S. Petrov. Phys. Rev. Lett. **103**, 153202 (2009).
[19] L. Pricoupenko and P. Pedri. Phys. Rev. A **82**, 033625 (2010).
[20] M. Taglieber, A.-C. Voigt, T. Aoki, T. W. Hänsch, and K. Dieckmann. Phys. Rev. Lett. **100**, 010401 (2008).
[21] E. Wille, F. M. Spiegelhalder, G. Kerner, D. Naik, A. Trenkwalder, G. Hendl, F. Schreck, R. Grimm, T. G. Tiecke, J. T. M. Walraven, S. J. J. M. F. Kokkelmans, E . Tiesinga, and P. S. Julienne. Phys. Rev. Lett. **100**, 053201 (2008).
[22] T. G. Tiecke, M. R. Goosen, A. Ludewig, S. D. Gensemer, S. Kraft, S. J. J. M. F. Kokkelmans, and J. T. M. Walraven. Phys. Rev. Lett. **104**, 053202 (2010).
[23] F. Spiegelhalder, A. Trenkwalder, D. Naik, G. Hendl, F. Schreck, and R. Grimm. Phys. Rev. Lett. **103**, 223203 (2009).
[24] M. Jag, M. Zaccanti, M. Cetina, R. S. Lous, F. Schreck, R. Grimm, D. S. Petrov, and J. Levinsen. Phys. Rev. Lett. **112**, 075302 (2014).
[25] see, e.g., G. Orso, L. P. Pitaevskii, and S. Stringari. Phys. Rev. A **77**, 033611 (2008).
[26] Instead of defining the reflection with respect to the y-axis, we could reflect with respect to the x-axis or any axis that lies in the xy-plane and goes through the origin.
[27] Y. Suzuki and K. Varga. *Stochastic Variational Approach to Quantum Mechanical Few-Body Problems*. Springer Verlag, Berlin (1998).
[28] J. Mitroy, S. Bubin, W. Horiuchi, Y. Suzuki, L. Adamowicz, W. Cencek, K. Szalewicz, J. Komasa, D. Blume, and K. Varga. Rev. Mod. Phys. **85**, 693 (2013).
[29] H. H. B. Sørensen, D. V. Fedorov, and A. S. Jensen, Nuclei and Mesoscopic Physics, ed. by V. Zelevinsky, AIP Conf. Proc. No. 777 (AIP, Melville, NY, 2005), p. 12.
[30] J. von Stecher and C. H. Greene. Phys. Rev. Lett. **99**, 090402 (2007).
[31] D. Rakshit, K. M. Daily, and D. Blume. Phys. Rev. A **85**, 033634 (2012).
[32] V. I. Kukulin and V. M. Krasnpol'sky. J. Phys. G **3**, 795 (1977).
[33] L. R. Dodd. Australian J. Phys. **25**, 507 (1972).
[34] O. I. Kartavtsev, A. V. Malykh, and S. A. Sofianos. J. of Experimental and Theoretical Phys. **108**, 365 (2009).
[35] N. P. Mehta. arXiv:1401.3314.
[36] V. N. Efimov. Yad. Fiz. **12**, 1080 (1970) [Sov. J. of Nucl. Phys. **12**, 589 (1971)].
[37] V. Efimov. JETP Lett. **16**, 50 (34) (1972).
[38] V. Efimov. Nucl. Phys. A **210**, 157 (1973).
[39] D. S. Petrov. Phys. Rev. A **67**, 010703(R) (2003).